



**HAL**  
open science

## Styryl-Functionalized Cage Silsesquioxanes as Nanoblocks for 3-D Assembly

Mathilde Laird, Arie van Der Lee, Dan Dumitrescu, Carole Carcel, Armelle Ouali, John Bartlett, Masafumi Unno, Michel Wong Chi Man

► **To cite this version:**

Mathilde Laird, Arie van Der Lee, Dan Dumitrescu, Carole Carcel, Armelle Ouali, et al.. Styryl-Functionalized Cage Silsesquioxanes as Nanoblocks for 3-D Assembly. *Organometallics*, 2020, 39 (10), pp.1896-1906. 10.1021/acs.organomet.0c00119 . hal-03095676

**HAL Id: hal-03095676**

**<https://hal.science/hal-03095676v1>**

Submitted on 4 Jan 2021

**HAL** is a multi-disciplinary open access archive for the deposit and dissemination of scientific research documents, whether they are published or not. The documents may come from teaching and research institutions in France or abroad, or from public or private research centers.

L'archive ouverte pluridisciplinaire **HAL**, est destinée au dépôt et à la diffusion de documents scientifiques de niveau recherche, publiés ou non, émanant des établissements d'enseignement et de recherche français ou étrangers, des laboratoires publics ou privés.

# New Functionalized Cage Silsesquioxanes as Nano Blocks for 3-D Assembly

Mathilde Laird<sup>†</sup>, Arie Van der Lee<sup>‡</sup>, Dan G. Dumitrescu<sup>§</sup>, Carole Carcel<sup>†</sup>, Armelle Ouali<sup>†</sup>, John R. Bartlett<sup>£\*</sup>, Masafumi Unno<sup>¥\*</sup> and Michel Wong Chi Man<sup>†\*</sup>

<sup>†</sup>ICGM, Univ Montpellier, CNRS, ENSCM, Montpellier, France

<sup>‡</sup>Institut Européen des Membranes, Université de Montpellier, UMR 5632 CNRS ENSCM, 34095 Montpellier, France

<sup>§</sup>XRD2 beamline, Elettra – Sincrotrone Trieste S.C.p.A., Strada Statale 14 – km 163,5 in AREA Science Park, 34149 Basovizza, Trieste, Italy

<sup>£</sup>Western Sydney University, Locked Bag 1797 Penrith NSW 2751 Australia

<sup>¥</sup>Department of Chemistry and Chemical Biology, Graduate School of Science and Technology, Gunma University, Kiryu 376-8515, Gunma, Japan.

*Supporting Information Placeholder*

---

**ABSTRACT:** Herein we report the synthesis of a new family of styryl-functionalized polyhedral oligomeric silsesquioxanes ( $T_n$ , where  $n = 8, 10$  and  $12$ ), in which the organic moiety is linked to all  $n$  vertices of the  $T_n$  cages via the phenyl ring rather than the vinyl group. In contrast to earlier studies in which the styryl group is linked to the cage via the vinyl moiety, our approach ensures that the vinyl moiety is less sterically hindered and available for post-functionalization. The functional  $T_n$  cages have been characterized by a range of techniques, including single crystal X-ray diffraction, multinuclear solution NMR ( $^1H$ ,  $^{13}C$  and  $^{29}Si$ ), MALDI-MS and FTIR. The solid-state structure of the  $T_8$  compound exhibited two non-equivalent  $Si_8O_{12}$  cage atoms, which has not been previously reported in the functionalized  $T_8$  system, although all cage atoms in the corresponding  $T_{10}$  and  $T_{12}$  systems were equivalent. In contrast, multinuclear solution NMR data indicated that all cages in the  $T_8$  system were equivalent in solution, suggesting that the non-equivalent cage geometries arise in the solid state to optimize the packing of the functionalized cages.

---

## 1. INTRODUCTION

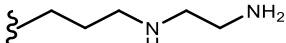
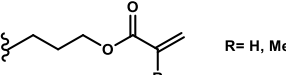
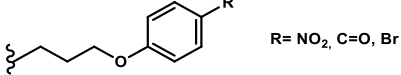
Since the early reports of their synthesis in the 1940s and 1950s<sup>1, 2</sup>, the development and characterization of oligomeric silsesquioxanes has been an area of significant activity within the materials and silicon chemistry communities. Of these, the polyhedral oligomeric silsesquioxanes (POSS,  $(R-SiO_{1.5})_n$ , where  $n=6, 8, 10, 12$ , etc.), also known as cage silsesquioxanes, have been of particular interest<sup>3, 4</sup>, with  $n=8$  being the most widely studied. These hybrid molecules, which are composed of a well-defined polyhedral core ( $(SiO_{1.5})_n$ ,  $T_n$ ) surrounded by organic moieties, can be readily incorporated into nanostructured materials either via hydrolysis-condensation processes involving silanol groups<sup>5</sup> or by polymerization on the organic moiety<sup>6-8</sup>. Self-organized systems<sup>9-11</sup>, templated POSS systems leading to mesoporous materials with  $T_8$  cages embedded with the walls<sup>12</sup>, and organic polymer-based nanohybrids<sup>13-18</sup> can all be obtained through judicious selection of functional organics. In addition, porous materials<sup>5, 6, 8</sup> in which the porosity can either arise from the voids between the cages or the core of the cage (0.3 nm)<sup>6</sup> have been reported. In general, the POSS core (e.g.  $T_8$ ) confers symmetry and thermal stability on the resulting materials, while the organic moieties provide flexibility and additional opportunities for functionalization. In addition, their well-defined structure gives them the advantage of a controlled proximity between adjacent branches. Since the distance

between silicon and oxygen is typically around 1.6 Å<sup>19, 20</sup>, the branches are separated by around 3 Å. This small spacing can lead to interesting cooperative effects and the suite of attractive POSS properties have been exploited in many fields including polymer chemistry<sup>13, 14, 21</sup>, bio/nanomedicine<sup>22-27</sup>, catalysis<sup>28-31</sup>, optical and sensing applications<sup>14, 32, 33</sup>, optoelectronics<sup>34</sup>, etc.

A significant majority of the applications described to date are based on functionalized  $T_8$  cages. Being often commercially available or easily synthesized, the latter can be produced in quantities of tens of grams for applications testing. In contrast, relatively few studies have described applications of larger cages<sup>35-39</sup>. The  $T_8$  cage has now been described with a wide range of substituents, including hydrido, methyl, octyl, phenyl, vinyl, chloropropyl, *etc*<sup>3</sup>. Larger cages are less common and are often obtained by cage rearrangement of pre-formed  $T_8$  species, as summarized in **Table 1**. Post-functionalization of pre-formed  $T_8$  materials can also produce a mixture of  $T_n$  species through rearrangement side-reactions (see, for example, entries 14-16 in **Table 1**). Functionalized  $T_n$  molecules bearing organic moieties that can be further modified via conventional, well-established reactions without modifying the structure of the  $T_n$  core, are of particular interest since they pave the way to an even wider range of potential applications. For example, organics bearing double bonds such as vinyl and styryl can be modified

using reactions such as hydrosilylation, Heck coupling, thiol-ene click reactions, hydrophosphination,

**Table 1. Selected T<sub>8</sub>, T<sub>10</sub> and T<sub>12</sub> cage silsesquioxane systems.**

Entry	Organic Group	Cages described	Synthesis type	Ref
1	Phenyl	T <sub>8</sub> , T <sub>10</sub> , T <sub>12</sub>	Direct synthesis basic/acidic conditions	40, 41
2	4-iodophenyl	T <sub>8</sub> , T <sub>10</sub> , T <sub>12</sub>	Rearrangement	
3	(4-Trimethylsilyl)benzene	T <sub>8</sub> , T <sub>10</sub> , T <sub>12</sub>	Post functionalization from phenyl cages	42
4	4-Nitrobenzene	T <sub>8</sub> , T <sub>10</sub> , T <sub>12</sub>	Direct synthesis (TBAF)	43
5	Vinyl	T <sub>8</sub> , T <sub>10</sub> , T <sub>12</sub>	Post functionalization	43
6	Vinyl	T <sub>8</sub> , T <sub>10</sub> , T <sub>12</sub>	Direct synthesis basic conditions	44, 45
7	Ethyl	T <sub>8</sub> , T <sub>10</sub> , T <sub>12</sub>	Post functionalization	44
8	Propyl, Butyl, Pentyl, Heptyl, Octyl, Nonyl, Decyl	T <sub>8</sub> , T <sub>10</sub>	Rearrangement	46
9	Chloropropyl	T <sub>8</sub> , T <sub>10</sub> , T <sub>12</sub>	Rearrangement	46
10	Bromopropyl, Iodopropyl	T <sub>8</sub> , T <sub>10</sub>	Rearrangement	46
11	Thiocyanopropyl	T <sub>8</sub> , T <sub>10</sub>	Rearrangement	46
12	(Pentafluorophenyl)propyl	T <sub>8</sub> , T <sub>10</sub>	Rearrangement	46
13		T <sub>8</sub> , T <sub>10</sub> , T <sub>12</sub>	Direct synthesis	47, 48
14	Azidopropyl	T <sub>8</sub> , T <sub>10</sub> , T <sub>12</sub>	Post functionalization chloropropyl and rearrangement	49
15	 R = H, Me	T <sub>8</sub> , T <sub>10</sub> , T <sub>12</sub>	Post functionalization chloropropyl and rearrangement	37
16	 R = NO <sub>2</sub> , C=O, Br	T <sub>8</sub> , T <sub>10</sub> , T <sub>12</sub>	Post functionalization chloropropyl and rearrangement	38
18	Vinyl <sub>n</sub> Phenyl <sub>12/10-n</sub>	T <sub>8</sub> , T <sub>10</sub> , T <sub>12</sub>	Rearrangement	50
19	Amino derivatives	T <sub>8</sub> , T <sub>10</sub>	Direct synthesis in acidic conditions	51

metathesis, polymerization, etc. In this context, the availability of T<sub>n</sub> precursors bearing styryl moieties grafted onto all “n” vertices would significantly extend the range of versatile POSS precursors. Octa-, deca- and dodeca-styrenyl cage silsesquioxanes have been synthesized from the corresponding vinyl-functionalized cage silsesquioxanes by cross-metathesis<sup>52-54</sup>, as illustrated in **Figure 1**. However, to the best of our knowledge, in all earlier reports, the vinylphenyl moiety is linked to the silsesquioxane cage via the vinylic C=C bond, which precludes further facile functionalization of the latter. An additional feature of the styryl-functionalized T<sub>n</sub> cages when compared to their vinyl analogues is that the phenyl group acts as a spacer, thus ensuring that the vinyl group is much less sterically hindered, and hence is more available for post-functionalization on all n vertices of the T<sub>n</sub> cage. In contrast, there have been several reports of mono-styryl-functionalized T<sub>8</sub> systems, in which one vertex bears a styryl function while the other seven vertices are linked to cyclopentyl<sup>15, 16, 55</sup>, cyclohexyl<sup>16</sup>, phenyl<sup>16</sup> or isobutyl<sup>16, 56</sup> moieties. A brief mention is made of potential applications for octastyryl-functionalized T<sub>8</sub> cages in the patent literature<sup>57</sup>, although no information regarding the synthesis or characterization of such precursors was disclosed.

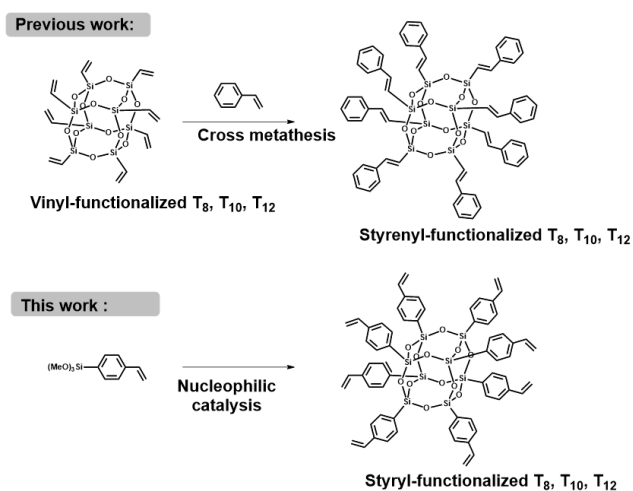


**Figure 1.** Structure of styrenyl (previous work) and styryl POSS precursors (current work), illustrating the accessibility of the “inner” and “peripheral” vinyl groups (for clarity, only the T<sub>8</sub> cages are shown).

In this work, we describe the synthesis and preparation of new octa-, deca and dodeca-styryl-silsesquioxanes, in which the styryl group is linked to the cage via the phenylene group. The

composition, structure and properties of these new precursors are also elucidated via single-crystal X-ray diffraction, NMR ( $^{29}\text{Si}$ ,  $^1\text{H}$  and  $^{13}\text{C}$ ) and IR spectroscopy, and structure/property correlations are described.

## 2. RESULTS AND DISCUSSION

### Synthesis

The approach used in our work to produce styryl-functionalized  $\text{T}_8$ ,  $\text{T}_{10}$  and  $\text{T}_{12}$  cage silsesquioxanes is based on a protocol developed by Bassindale's group<sup>58</sup>, as shown in **Figure 2**. This approach, which has not been widely employed, typically provides better yields than alternative approaches involving hydrolysis of chlorosilane or ethoxysilane precursors, which often exhibit relatively low yields<sup>59, 60</sup>. It also avoids the production of large quantities of corrosive HCl typically produced when using chlorosilanes, which can lead to difficulties in controlling the rates of hydrolysis and condensation. It has been demonstrated that the reaction can be used with a variety of organotrialkoxysilanes to produce  $\text{T}_8$  cage silsesquioxanes functionalized with the corresponding organic group, including alkyl, cyclopentyl, cyclohexyl, *i*-butyl, phenyl, etc<sup>58, 61</sup>. However, the water content must be carefully controlled<sup>58, 61</sup> since it plays an important role in the catalyzed synthesis. During our preliminary experiments to optimize the synthesis conditions for producing styryl-functionalized cage silsesquioxanes, using both base- and fluoride-catalyzed conditions, the use of TBAF emerged as the preferred approach. In particular, base-catalyzed reactions led mainly to polymers and mixtures of cages which could not be identified.

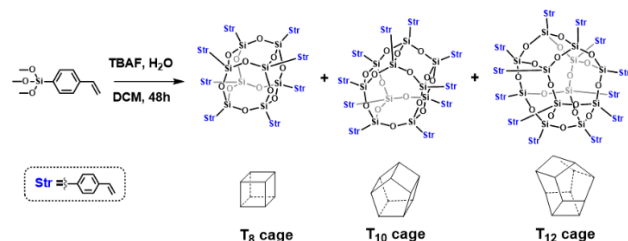


**Figure 2.** Synthesis of styryl-functionalized  $\text{T}_8$ ,  $\text{T}_{10}$  and  $\text{T}_{12}$  cage silsesquioxanes.

When using fluoride as a catalyst, the temperature, concentration of fluoride and the quantity of water present have been identified as key parameters for controlling the reaction<sup>58</sup>. However, large amounts of water were reported to lead to the formation of partially condensed cage silsesquioxanes or silanols<sup>61</sup>. In the work of Bassindale's group, the water involved in the hydrolysis-condensation process was that naturally associated with the commercially available hydrophilic TBAF. Although our approach was largely inspired by this earlier work<sup>58</sup>, the reaction described herein involves the use of greater quantities of water than that initially associated with the TBAF. Indeed, we observed that in the case of styryl trimethoxysilane as precursor, fewer by-products were obtained by adding one equivalent of water per silicon.

The reaction was thus carried out using a commercially available styryltrimethoxysilane with TBAF and water in DCM for two days (see Experimental). The crude reaction product was treated with anhydrous  $\text{CaCl}_2$  and washed with water to

**Table 3.** Characteristic bond distances and angles for styryl-functionalised  $\text{T}_8$  and  $\text{T}_{10}$  cage silsesquioxanes

remove excess TBAF. Preliminary characterization by  $^1\text{H}$  and  $^{29}\text{Si}$  solution NMR revealed the presence of a mixture of  $\text{T}_8$ ,  $\text{T}_{10}$  and  $\text{T}_{12}$  cage silsesquioxanes as the main products (based on a comparison with the chemical shifts previously reported for other functionalized  $\text{T}_8$ ,  $\text{T}_{10}$  and  $\text{T}_{12}$  species, **Table 2**), together with larger cages and partially condensed products that could not be readily identified. Analysis of the integrated intensity of signals in the  $^1\text{H}$  NMR spectrum revealed that the  $\text{T}_8$ ,  $\text{T}_{10}$  and  $\text{T}_{12}$  products were present in a 1:3:1 mole ratio, with the functionalized  $\text{T}_{10}$  silsesquioxane being the main reaction product. After recrystallization and column chromatography,  $\text{T}_8$ ,  $\text{T}_{10}$  and  $\text{T}_{12}$  compounds were obtained separately and characterized.

**Table 2.** Typical  $^{29}\text{Si}$  NMR chemical shifts reported for functionalised  $\text{T}_8$ ,  $\text{T}_{10}$  and  $\text{T}_{12}$  cage silsesquioxanes.

Organic group	$\text{T}_8$ shift (ppm)	$\text{T}_{10}$ shift (ppm)	$\text{T}_{12}$ shifts (ppm)	Ref.
Styryl	-78.19	-79.59	-79.45, -81.29	This work <sup>51, 62</sup>
Phenyl	-78.3	-79.6	n.a.	44
4-Methylbenzene	-78.0	-79.6	n.a.	44
4-Nitrobenzene	-79.2	-80.9	-80.3, -82.2	44
4-Trimethylsilylbenzene	-78.4	-79.5	-79.4, -81.5	44
Azidopropyl	-67.0	-68.9	-68.7, -71.4	37
Propylmethacrylate	-66.8	-68.6	-68.4, -71.1	38
4-(nitrobenzene) propoxy	-68.7	-68.6	-68.3, -71.0	39

### Mass Spectrometry

The MALDI TOF mass spectra of the styryl-functionalized  $\text{T}_8$ ,  $\text{T}_{10}$  and  $\text{T}_{12}$  (**Figures S1, S2 and S3**, respectively) exhibited peaks at 1263.1, 1573.2 and 1884.1 m/z, which were attributed to  $\text{T}_8+\text{Na}$ ,  $\text{T}_{10}+\text{Na}$  and  $\text{T}_{12}+\text{Na}$ , respectively (expected m/z = 1263.2, 1573.2 and 1883.3). These are each separated by 310 m/z, arising from the addition of [styryl-SiO<sub>1.5</sub>]<sub>2</sub> moieties with each increment in n.

### Single Crystal X-ray Structures

Fractional recrystallization in a mixture of toluene and pentane enabled crystals suitable for X-ray diffraction measurements to be obtained. The crystal structures were solved using the ab-initio iterative charge flipping method (see **Experimental**). The space group symmetry of the crystal structures of  $\text{T}_8$ ,  $\text{T}_{10}$  and  $\text{T}_{12}$  were  $P2_1/n$ ,  $R-3c$  and  $P4/ncc$ , respectively. **Table S1** summarizes the structural parameters for the  $\text{T}_8$ ,  $\text{T}_{10}$  and  $\text{T}_{12}$  cages.

The structure of the styryl-functionalized  $\text{T}_8$  system is illustrated in **Figures 3 and S4**, while the minimum, maximum and average values of the characteristic bond lengths and angles are presented in **Table 3**. The values measured are similar to those of the octaphenyl-functionalized  $\text{T}_8$  cage<sup>19, 63</sup> and are typical for bond distances and angles in the octasilsesquioxane

	Styryl T <sub>8</sub>			Styryl T <sub>10</sub>		
	min	average	max	min	average	max
Si-O (Å)	1.603	1.617	1.631	1.598	1.610	1.629
Si-C (Å)	1.827	1.841	1.852	1.810	1.829	1.850
Si-O-Si (°)	138.6	149.1	161.5	145.3	152.6	161.1
O-Si-O (°)	107.5	109.1	110.2	107.0	109.2	111.0

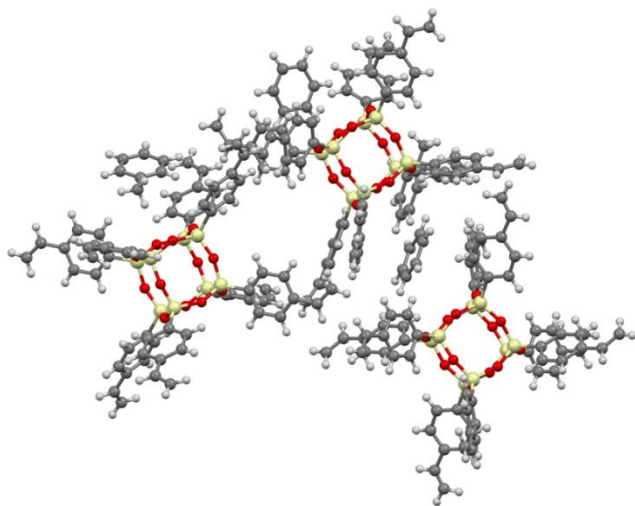


**Figure 3.** X-ray crystal structure of styryl-functionalized T<sub>8</sub> cage silsesquioxane.

family: Si-O bond length (1.55 to 1.65 Å; average = 1.60 Å); Si-O-Si angle (145 to 152 °; average = 148.5 °); O-Si-O angle (107 to 112 °; average = 109 °)<sup>58</sup>. However, it is evident, as illustrated in **Figure S5**, that two inequivalent T<sub>8</sub> cages are found in the lattice. To the best of our knowledge, such a phenomenon has not been previously observed in the functionalized T<sub>8</sub> system, and we conclude that the different geometries are adopted to optimize the packing of the molecules in the solid state. In addition, three toluene molecules, from the solvent used for the crystallization, and one benzene molecule are present in the refined structure. Although the expected methyl group was not identified in the difference Fourier maps, the additional solvent molecule is undoubtedly toluene, since no benzene was used in the synthesis. This apparent anomaly is attributed to rotational disorder in the solvent retained within the crystals, which leads to the electron density of the carbon being delocalized over more than one position. In addition, the asymmetric part of the unit cell contains one complete T<sub>8</sub> cluster and two half T<sub>8</sub> clusters, with the latter two clusters located on inversion centers. The packing of the aromatic rings (**Figure S4**) highlights the interactions between the styryl functions on adjacent cages, although there is no evidence of

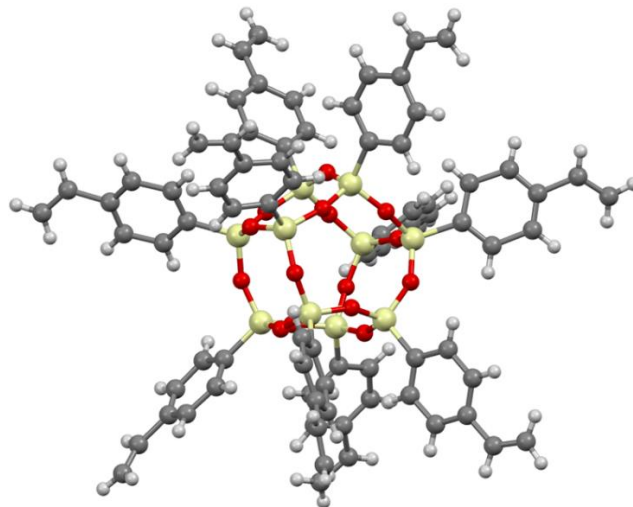


**Figure 4.** X-ray crystal structure of styryl-functionalized T<sub>10</sub> cage silsesquioxane.

extended  $\pi$ - $\pi$  interactions. Nevertheless, these interactions, coupled with the rigidity provided by the phenyl rings, are sufficient to ensure that the compound is a solid at room temperature. As observed in earlier studies, at ambient temperature, functionalized T<sub>8</sub> molecules that can interact through  $\pi$ - $\pi$  interactions or formation of liquid-crystalline domains<sup>61</sup> are typically solids, whereas those that cannot pack uniformly (such as isoocetyl<sup>61</sup>, n-propylacrylate<sup>37</sup>, etc) are often liquids or oils.

The X-ray crystal structure of the styryl-functionalized T<sub>10</sub> cage is presented in **Figures 4** and **S6** and the values of the characteristic bond lengths and angles are gathered in **Table 3**. Only a small number of single crystal structures of functionalized T<sub>10</sub> systems have previously been reported<sup>64-66</sup>, compared to the T<sub>8</sub> system for which a large number of compounds have been comprehensively characterized. In contrast to the corresponding T<sub>8</sub> system, only one unique cage geometry was identified for styryl-functionalized T<sub>10</sub>, consistent with previous reports of the structures of functionalized T<sub>10</sub> moieties. Most vinyl groups on the T<sub>10</sub> surface were poorly resolved in the electron density map and hence the fragments were modelled with soft distance restraints on the double and single bonds. The distances used for this modelling were taken from the Cambridge Structural Database<sup>67</sup> and the latter were thermally restrained. Large solvent-accessible voids appeared in the structure in which no fragments could be recognized.

Given the relatively small number of T<sub>10</sub> systems previously characterized, it is of interest to compare the structure of the

styryl-functionalized  $T_{10}$  with that of other systems, and representative structural data is presented in **Table S2**. The Si-O bond lengths vary from 1.600 to 1.618 Å (average 1.607 Å) in the two five-silicon rings and from 1.598 to 1.629 Å (average 1.611 Å) in the five four-silicon rings and hence the cage deviates from ideal  $D_{5h}$  symmetry. Similar deviations from symmetry have also been reported for the H- $T_{10}$  system<sup>65</sup> (**Table S2**), although they are much smaller in the latter case. The variations in Si-O-Si bond angles in both the five-silicon and four-silicon rings are also significantly greater in the styryl-functionalized system, although the average values are comparable.

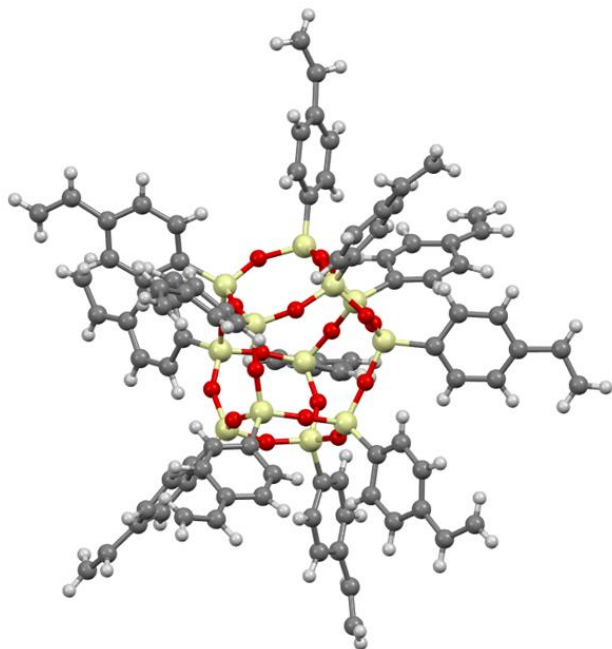


**Figure 5.** X-ray crystal structure of styryl-functionalized  $T_{12}$  cage silsesquioxane.

The single-crystal X-ray structure of the styryl-functionalized  $T_{12}$  compound is illustrated in **Figures 5** and **S7**, while the minimum, maximum and average values of the characteristic bond lengths and angles are compared to those of other reported  $T_{12}$  compounds in **Table 4**. Two possible isomers have been proposed for  $T_{12}$  cage silsesquioxanes, one of which is highly symmetrical ( $D_{6h}$  point-group symmetry) while the other is less-symmetrical ( $D_{2d}$  symmetry), as illustrated in **Figure 6**. In the current work, and consistent with earlier reports<sup>37, 38, 43, 47, 49</sup>, it is evident that the less-symmetrical isomer is obtained in our work, in which silicon atoms are part of either (a) one five-silicon-atom-ring and two four-silicon-atom-rings ( $5^14^2$ , following the notation used by Agaskar et al.<sup>59, 68</sup>; four vertices marked with red spheres in **Figure 6**); or (b) two five-silicon-atom rings and one four-silicon-atom ring ( $5^24^1$ ; eight vertices marked with blue spheres in **Figure 6**). The average Si-O bond lengths and O-Si-O bond angles are comparable to those observed for other  $T_{12}$  compounds (**Table 4**). However, the average Si-O-Si bond angle is somewhat larger in the case of the styryl-functionalized  $T_{12}$  cage than is observed for the corresponding hydrido- or Ph-functionalized compounds, due mainly to the presence of two unusually large angles of 178°. Similar features are also observed in the case of the *p*-iodophenyl-functionalized  $T_{12}$  cage<sup>42</sup>, although not for the phenyl-functionalized

compound<sup>20</sup>. This suggests that the cage structure might distort to accommodate the bulky *para* substituents in the solid state.

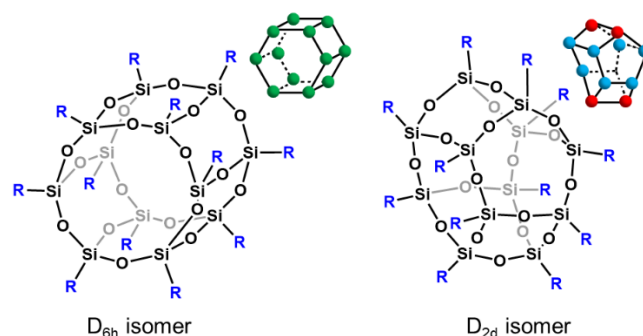


**Figure 6.** Possible isomers observed in the  $T_{12}$  cage silsesquioxane system. Left,  $D_{6h}$  isomer; right,  $D_{2d}$  isomer (R = styryl).

**Table 4. Characteristic bond lengths and bond angles in functionalized  $T_{12}$  cage silsesquioxanes.**

	(Styr) <sub>12</sub> T <sub>12</sub> (This work)	H <sub>12</sub> T <sub>12</sub> (Ref. <sup>69</sup> )	Ph <sub>12</sub> T <sub>12</sub> (Ref. <sup>20</sup> )	( <i>p</i> -I-Ph) <sub>12</sub> T <sub>12</sub> (Ref. <sup>42</sup> )
Si-O (Å)	1.56-1.66 (av=1.60)	1.58-1.62 (av=1.60)	1.60-1.62 (av=1.61)	1.59-1.62 (av=1.61)
Si-C (Å)	1.78-1.87 (av=1.82)		1.84-1.85 (av=1.842)	1.83-1.85 (av=1.840)
Si-O-Si (°)	149-178 (av=160)	143-164 (av=155)	145-158 (av=151)	146-173 (av=157)
O-Si-O (°)	107-112 (av=109)	108-111 (av=110)	107-111 (av=109)	107-111 (av=109)

#### NMR Characterization

<sup>1</sup>H, <sup>13</sup>C and <sup>29</sup>Si solution NMR spectroscopy were used to further characterize the structure of the styryl-functionalized  $T_8$ ,  $T_{10}$  and  $T_{12}$  cages in solution, and to compare the solution speciation with that observed in the solid state via X-ray diffraction. The styryl- $T_8$  <sup>1</sup>H NMR spectrum (**Figure 7**) shows characteristic signals at 7.71 (doublet) and 7.40 ppm (doublet) arising from the aromatic ring, together with clusters at 6.70 (doublet of doublets), 5.80 (doublet) and 5.28 ppm (doublet) associated with the vinylic moiety, with the expected 2:2:1:1 intensity ratios. The corresponding signals in the case of the styryl- $T_{10}$  silsesquioxane move upfield to 7.56 and 7.29 ppm for the aromatic protons, although the positions of the signals arising from the vinylic protons (6.66 ppm, 5.76 ppm and 5.27 ppm) vary to a lesser extent than those of the aromatic signals (**Table 5**). A similar phenomenon has also been observed in the case of the phenyl-functionalized  $T_8$  and  $T_{10}$ , with reported resonances at 7.75, 7.42 and 7.36 ppm for the  $T_8$  system<sup>70</sup> and 7.57, 7.33 and 7.20 ppm for the corresponding  $T_{10}$  system for the aromatic protons<sup>42</sup>. This phenomenon is attributed to the increased rotational freedom of the styryl group, which is sterically less hindered on the five-silicon-atom rings of the  $T_{10}$ .

The <sup>1</sup>H-NMR spectrum of the styryl-functionalized  $T_{12}$  system (**Figure 7**) reflects the presence of two different silicon sites in



the T<sub>12</sub> cage (**Figure 6**). As expected, the four styryl groups linked to 5<sup>1</sup>4<sup>2</sup> and the eight styryl groups linked to 5<sup>2</sup>4<sup>1</sup> sites each give rise to distinct clusters of NMR signals, with the expected 1:2 integrated intensity ratio being observed (**Figure 7**). The observed chemical shifts are compared to those observed for 4<sup>3</sup> and 5<sup>1</sup>4<sup>2</sup> silicons in the corresponding T<sub>8</sub> and T<sub>10</sub> compounds, respectively, in **Table 5**. These data clearly highlight the impact of T<sub>n</sub> ring strain on the observed chemical shifts of the phenyl-ring protons, with increasing ring strain leading to a corresponding downfield movement in the position of the <sup>1</sup>H resonances. In contrast, those of the vinyl moiety are less impacted, although a small downfield movement is still observed.

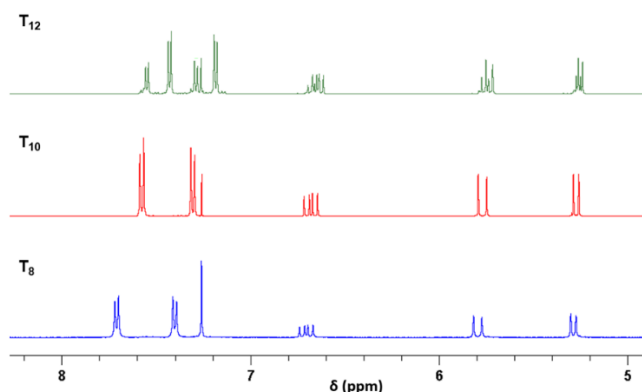
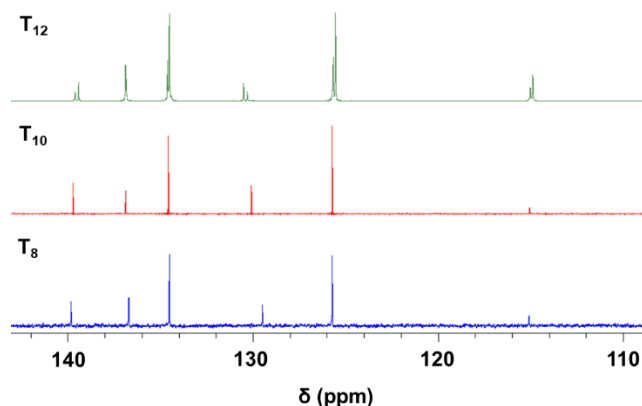


**Figure 7.** <sup>1</sup>H NMR spectra of styryl-functionalized T<sub>8</sub>, T<sub>10</sub> and T<sub>12</sub> cage silsesquioxanes (CDCl<sub>3</sub>).

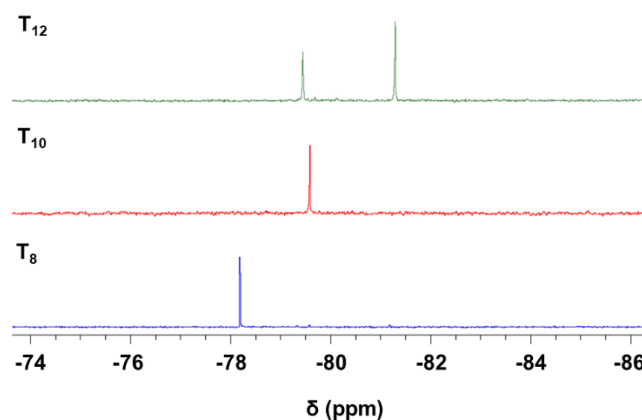
<sup>13</sup>C NMR (**Figure 8**) reveals similar spectra for the three structures, with the assignments of signals associated with each carbon atom given in **Table 6**. Each of the two populations of non-equivalent silicon sites in the T<sub>12</sub> cage gives rise to a separate set of signals, as expected. As few details are available in the literature concerning the influence of the type of cage on the observed <sup>13</sup>C NMR signals, further interpretation and comparison of the spectra is difficult, with no systematic trends being evident.

In <sup>29</sup>Si NMR, as indicated above, the compounds exhibit different chemical shifts. The T<sub>8</sub> and T<sub>10</sub> silsesquioxane cages both feature geometries in which all silicon atoms are equivalent, and hence a single sharp signal would be expected for each of these cage silsesquioxanes. The silicon atoms belonging to the three 4-silicon-atom rings (4<sup>3</sup>) of the T<sub>8</sub> cage exhibit a single signal at -78.19 ppm (**Figure 9** and **Table 2**). In contrast, silicon atoms of the T<sub>10</sub> structure belonging to one 5-silicon-atom ring and two 4-silicon-atom rings (5<sup>1</sup>4<sup>2</sup>) are observed at a significantly different chemical shift compared to the signal from the corresponding T<sub>8</sub> structure. In particular, the T<sub>10</sub> spectrum yields a single signal at -79.59 ppm (**Figure 9** and **Table 2**). Changing from a 4-silicon ring to a 5-silicon ring results in a decrease of the ring strain<sup>3, 46, 51</sup>, and to a corresponding upfield shift in the position of the <sup>29</sup>Si signal. This effect has now been confirmed in multiple cases for such cage silsesquioxanes (**Table 2**)<sup>37, 38, 41, 47, 49, 51</sup>, including the phenyl-functionalized T<sub>8</sub> and T<sub>10</sub> systems for which the <sup>29</sup>Si signal is observed at -78.30<sup>70</sup> and -79.60 ppm<sup>51</sup>, respectively.

**Table 5.** <sup>1</sup>H NMR chemical shifts in the solution NMR spectra of styryl-functionalised T<sub>8</sub>, T<sub>10</sub> and T<sub>12</sub> cage silsesquioxanes (d, doublet; dd, doublet of doublets; m, multiplet).



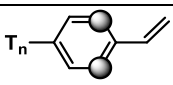
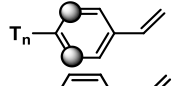
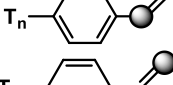
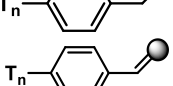
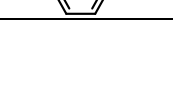
**Figure 8.** <sup>13</sup>C NMR spectra of styryl-functionalized T<sub>8</sub>, T<sub>10</sub> and T<sub>12</sub> cage silsesquioxanes (CDCl<sub>3</sub>).



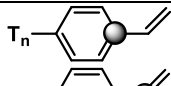
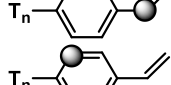
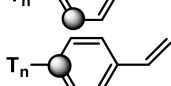
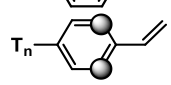
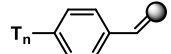
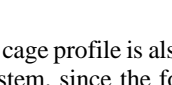
**Figure 9.** <sup>29</sup>Si NMR spectra of styryl-functionalized T<sub>8</sub>, T<sub>10</sub> and T<sub>12</sub> cage silsesquioxanes (CDCl<sub>3</sub>).

It is also of interest to recall that single-crystal X-ray diffraction studies revealed the presence of two non-equivalent Si<sub>8</sub>O<sub>12</sub> cages in the styryl-functionalized T<sub>8</sub> system (**Figure S5**), although only one cage type was identified in the corresponding T<sub>10</sub> system. In contrast, the NMR data suggest that only a single cage structure is present in solution for both systems. This suggests that the packing constraints that imposed the T<sub>8</sub> deformation in the solid state are relaxed in solution leading to a single silicon environment, and hence, to a single signal in the corresponding <sup>29</sup>Si solution NMR spectrum.

The <sup>29</sup>Si NMR spectrum of the styryl-functionalized T<sub>12</sub> POSS is compared to those of the corresponding T<sub>8</sub> and T<sub>10</sub> compounds in **Figure 9**. Whereas the T<sub>8</sub> and T<sub>10</sub> compounds exhibit only single signals, the T<sub>12</sub> cage exhibits two signals at -79.45 and -81.29 ppm. As indicated above, earlier work relating the effect of ring strain in 4- and 5-silicon-atom rings to the position of the <sup>29</sup>Si NMR resonance concluded that the former is more strained than the latter<sup>3, 51</sup>, leading to a corresponding downfield shift in the position of the resonance. On this basis, the <sup>29</sup>Si signal at -79.45 ppm is assigned to 5<sup>1</sup>4<sup>2</sup> silicon atoms, while that observed at -81.29 ppm is assigned to 5<sup>2</sup>4<sup>1</sup> silicon atoms.

Chemical shift (ppm)			Assignment
T <sub>8</sub>	T <sub>10</sub>	T <sub>12</sub>	
7.70 – 7.72 (d)	7.55 – 7.57 (d)	7.55 – 7.53 (d) 7.43 – 7.41 (d)	
7.39 – 7.41 (d)	7.28 – 7.30 (d)	7.29 – 7.28 (d) 7.19 – 7.17 (d)	
6.67 – 6.74 (dd)	6.63 – 6.70 (dd)	6.67 – 6.60 (m)	
5.77 – 5.82 (dd)	5.74 – 5.78 (dd)	5.75 – 5.70 (m)	
5.27 – 5.30 (dd)	5.25 – 5.28 (dd)	5.25 – 5.23 (m)	

**Table 6.** <sup>13</sup>C NMR chemical shifts in the solution NMR spectra of styryl-functionalised T<sub>8</sub>, T<sub>10</sub> and T<sub>12</sub> cage silsesquioxanes.

Chemical shift (ppm)			Assignment
T <sub>8</sub>	T <sub>10</sub>	T <sub>12</sub>	
139.9	139.7	139.6-139.4	
136.8	136.8	136.9-136.8	
134.6	134.6	134.6-134.5	
129.6	130.1	130.5-130.3	
125.8	125.7	125.6-125.5	
115.2	115.0	115.0-114.9	

### IR Characterization

The FTIR spectra of the styryl-functionalized T<sub>8</sub>, T<sub>10</sub> and T<sub>12</sub> compounds are included in **Figure S8**, while the corresponding band positions and assignments are summarized in **Table S3**. All peak positions and full-widths at half-maximum (FWHM) were obtained by fitting the spectral profiles with a cubic spline baseline function together with Gaussian functions for the individual peaks. The spectra exhibit the typical features expected for cage silsesquioxanes and styryl moieties and peaks may be broadly assigned on the basis of the vibrational modes expected for these respective chemical groups. Only minor differences are evident in the positions and FWHM of peaks arising from the styryl species in the T<sub>8</sub>, T<sub>10</sub> and T<sub>12</sub> systems, suggesting that the local environments of the styryl species and relative orientations of the phenyl ring and vinyl group are similar in all three systems.

It is evident from **Figure S8** that the spectral profile of the T<sub>8</sub> cage (with exclusively 4<sup>3</sup> silicon sites) is somewhat broader than that of the T<sub>10</sub> system (with only 5<sup>1</sup>4<sup>2</sup> silicon sites). This might arise either from the presence of two non-equivalent cages in the solid state (to optimize the packing of the molecules, as identified by single crystal XRD), and/or the higher Si-O bond strain in the T<sub>8</sub> system (see above), leading to broader

peak profiles. Similarly, the T<sub>12</sub> cage profile is also significantly broader than that of the T<sub>10</sub> system, since the former contains two non-equivalent silicon sites (5<sup>1</sup>4<sup>2</sup> and 5<sup>2</sup>4<sup>1</sup>), resulting in a more complex profile with overlapping peaks.

### 3. CONCLUSIONS

In summary, we report the synthesis and characterization of three new styryl-functionalized T<sub>n</sub> cage silsesquioxanes (T<sub>8</sub>, T<sub>10</sub> and T<sub>12</sub>) in which styryl groups are linked to all n vertices of the T<sub>n</sub> compounds via the phenyl groups. A key feature of the styryl-functionalized T<sub>n</sub> cages when compared to their vinyl-functionalized analogues is that the phenyl group acts as a spacer, thus ensuring that the vinyl group of the styryl is much less sterically hindered, and hence is more available for post-functionalization on all n vertices of the T<sub>n</sub> cage.

The T<sub>8</sub> compound exhibits non-equivalent Si<sub>8</sub>O<sub>12</sub> cages in the solid state, with the different geometries being adopted to optimize the packing of the molecules in the solid state. In contrast, only single populations of Si<sub>n</sub>O<sub>3n/2</sub> cages are evident in the corresponding T<sub>10</sub> and T<sub>12</sub> solid-state systems. In all three cases, multinuclear solution NMR studies (<sup>1</sup>H, <sup>13</sup>C and <sup>29</sup>Si) indicated



that single populations of symmetrical, well-defined cages (with ideal  $O_h$ ,  $D_{5h}$  and  $D_{2d}$  symmetries for  $T_8$ ,  $T_{10}$  and  $T_{12}$  cages, respectively) were present.

As a consequence of the lower steric hindrance of the vinyl sites on these new cage silsesquioxanes compared to those of previously reported vinyl-functionalized analogues, we envisage that these new precursors will serve as building blocks for producing nano-structured materials with potential application in diverse fields. The synthesis of such materials will be explored in future studies.

## 4. EXPERIMENTAL SECTION

**4.1 Chemicals and purification methods.** Tetrabutylammonium fluoride (TBAF, 1 M solution in THF (containing 5%  $H_2O$ ), (4-vinylphenyl)trimethoxysilane and dichloromethane (DCM, Analytical Grade) were obtained from Sigma Aldrich, TCI and VWR, respectively, and were used without further purification. All syntheses were undertaken using HPLC-quality water.

The products obtained were purified by recrystallization in toluene/pentane (VWR, normapur and pure 95%, respectively) and by flash chromatography in a Buchi Reveleris X2 flash chromatography system, equipped with evaporative light-scattering detection (ELSD) and 254-nm light source, using a mixture of DCM/cyclohexane (VWR, technical grade).

**4.2 Silsesquioxane cage synthesis.** In a round bottom flask, a solution of trimethoxy(4-vinylphenyl)silane (3.7 mL, 17.5 mmol) in DCM (400 mL) was prepared. Water (160  $\mu$ L, 8.75 mmol) was added to the previous solution, followed by the dropwise addition of the TBAF solution in THF (10 mL, 10 mmol). The reaction mixture was held at 30 °C for 48 h. Anhydrous  $CaCl_2$  (1.2 g, 11 mmol) was added to the solution and suspended for 16 h. The resulting crude product was filtered, washed three times with water (300 mL aliquots), and dried over  $Na_2SO_4$ . The solvent was then evaporated under reduced pressure. The crude reaction product contained  $T_8$ ,  $T_{10}$  and  $T_{12}$  cage silsesquioxanes (as revealed by  $^1H$  NMR) which were fractionally recrystallized in a mixture of toluene/pentane to obtain  $T_8$ ,  $T_{10}$  and  $T_{12}$  crystals. The supernatant was then evaporated and the resulting solid purified by flash column chromatography with DCM/cyclohexane 20/80 (by volume) to obtain the remaining styryl-functionalized  $T_8$ ,  $T_{10}$  and  $T_{12}$  products.

**Octastyryl silsesquioxane** (white powder): Yield: 11.8%.  $^1H$  NMR (400 MHz,  $CDCl_3$ ,  $\delta$ , ppm): 7.71 (d,  $CH_{ar}$ , 16H,  $J = 8.1$  Hz), 7.40 (d,  $CH_{ar}$ , 16H,  $J = 8.1$  Hz), 6.70 (dd,  $CH_{vi}$ , 8H,  $J_1 = 17.6$  Hz,  $J_2 = 11.4$  Hz), 5.80 (d,  $CH_{vi}$ , 8H,  $J_1 = 17.6$  Hz,  $J_2 = 0.8$  Hz), 5.28 (d,  $CH_{vi}$ , 8H,  $J_1 = 11.4$  Hz,  $J_2 = 0.8$  Hz).  $^{13}C$  NMR (100 MHz,  $CDCl_3$ ,  $\delta$ , ppm): 139.92 ( $C_{ar}$ ), 136.76 ( $C_{vi}H$ ), 134.59 ( $C_{ar}H$ ), 129.56 ( $C_{ar}$ ), 125.81 ( $C_{ar}H$ ), 115.19 ( $C_{vi}H_2$ ).  $^{29}Si$  NMR (80 MHz,  $CDCl_3$ ,  $\delta$ , ppm): -78.19. MALDI-MS: m/z: calculated for  $C_{64}H_{56}O_{12}Si_8$  (M+Na): 1263.18; found: 1263.14.

**Decastyryl silsesquioxane** (white powder): Yield: 9.8%.  $^1H$  NMR (400 MHz,  $CDCl_3$ ,  $\delta$ , ppm): 7.56 (d,  $CH_{ar}$ , 20H,  $J = 8.3$  Hz), 7.29 (d,  $CH_{ar}$ , 20H,  $J = 8.3$  Hz), 6.66 (dd,  $CH_{vi}$ , 10H,  $J_1 = 17.6$  Hz,  $J_2 = 10.8$  Hz), 5.76 (d,  $CH_{vi}$ , 10H,  $J_1 = 17.6$  Hz,  $J_2 = 0.9$  Hz), 5.27 (d,  $CH_{vi}$ , 10H,  $J_1 = 10.8$  Hz,  $J_2 = 0.9$  Hz).  $^{13}C$  NMR (100 MHz,  $CDCl_3$ ,  $\delta$ , ppm): 139.70 ( $C_{ar}$ ), 136.83 ( $C_{vi}H$ ), 134.55 ( $C_{ar}H$ ), 130.05 ( $C_{ar}$ ), 125.70 ( $C_{ar}H$ ), 115.04 ( $C_{vi}H_2$ ).  $^{29}Si$  NMR (80 MHz,  $CDCl_3$ ,  $\delta$ , ppm): -79.59. MALDI-MS: m/z: calculated for  $C_{80}H_{70}O_{15}Si_{10}$  (M+Na): 1573.23; found: 1573.24.

**Dodecastyryl silsesquioxane** (white powder): Yield: 2.5%.  $^1H$  NMR (400 MHz,  $CDCl_3$ ,  $\delta$ , ppm): 7.54 (d,  $CH_{ar}$ , 8H,  $J = 8.0$  Hz),

7.42 (d,  $CH_{ar}$ , 16H,  $J = 8.1$  Hz), 7.29 (d,  $CH_{ar}$ , 8H,  $J = 8.0$  Hz), 7.18 (d,  $CH_{ar}$ , 16H,  $J = 8.1$  Hz), 6.69 (m,  $CH_{vi}$ , 12H), 5.78 (m,  $CH_{vi}$ , 12H), 5.24 (m,  $CH_{vi}$ , 12H).  $^{13}C$  NMR (100 MHz,  $CDCl_3$ ,  $\delta$ , ppm): 139.59 ( $C_{ar}$ ), 139.39 ( $C_{ar}$ ), 136.86 ( $C_{vi}H$ ), 136.82 ( $C_{vi}H$ ), 134.59 ( $C_{ar}H$ ), 134.48 ( $C_{ar}H$ ), 130.48 ( $C_{ar}$ ), 130.28 ( $C_{ar}$ ), 125.64 ( $C_{ar}H$ ), 125.52 ( $C_{ar}H$ ), 115.00 ( $C_{vi}H_2$ ), 114.87 ( $C_{vi}H_2$ ).  $^{29}Si$  NMR (80 MHz,  $CDCl_3$ ,  $\delta$ , ppm): -79.45, -81.29. MALDI-MS: m/z: calculated for  $C_{96}H_{84}O_{18}Si_{12}$  (M+Na): 1884.3; found: 1884.1.

**4.3 Characterization methods.** FTIR spectra were recorded from 650 to 4000  $cm^{-1}$  using a PerkinElmer Spectrum 100 equipped with a Gladia-ATR accessory. The spectral profiles were fitted with Gaussian functions using the Fityk software package (Version 1.3.1, freeware downloaded from <http://fityk.nieto.pl>).

MALDI-MS spectra were acquired using a Bruker Rapiflex spectrometer with dithranol/sodium trifluoroacetate as desorption matrix.

Liquid  $^1H$ ,  $^{13}C$  and  $^{29}Si$  NMR spectra were recorded on a Bruker Avance 400 MHz spectrometer in  $CDCl_3$  at room temperature and at concentrations of around 10 mg/mL. All  $^{29}Si$  and  $^{13}C$  spectra were proton decoupled and chemical shifts ( $\delta$ ) were calibrated against the signal of tetramethylsilane as internal standard.

Single crystal X-ray diffraction data for the styryl-functionalized  $T_8$  and  $T_{10}$  compounds were obtained on a Rigaku Oxford Diffraction Gemini-S diffractometer with sealed-tube Mo- $K\alpha$  radiation using the CrysAlis Pro program (Rigaku Oxford Diffraction, 2017). The data collections were carried out at 175 K. The integration of the data frames was done with the same program using default parameters. Lorentz and polarization effects were also corrected, and the empirical absorption correction was done using spherical harmonics employing symmetry-equivalent and redundant data. The crystal evaluation and data collection for the styryl-functionalized  $T_{12}$  was carried out at the XRD1 beamline of the Elettra synchrotron (Lausi et al <sup>71</sup>) on a serial Huber kappa goniometer at a wavelength of  $\lambda = 0.7000$  Å. Frame integration and scale and absorption corrections were done with XDS (Kabsch <sup>72</sup>) and space group assignment was provided by Pointless from the CCP4 software suite (Winn et al <sup>73</sup>). Because of the very weak scattering, a data collection for five different crystals was done, and the best data set was selected for structure solution and refinement. The maximum data resolution was not better than 1.1 Å, but the structure could immediately be solved by dual space methods.

The crystal structures were solved using the ab-initio iterative charge flipping method with parameters described by Van der Lee <sup>74</sup> and using the Superflip program <sup>75, 76</sup>. The structural models were refined against  $|F|$  using full-matrix non-linear least-squares procedures as implemented in CRYSTALS <sup>76</sup> on all independent reflections with  $I > 2\sigma(I)$ . Complete data were collected up to 1 Å resolution, because data beyond that resolution were mostly below the  $2\sigma(I)$  threshold.

When the vinyl groups on the cluster surface of the structure ( $T_8$ ) were poorly identified in the electron density map, the fragments were modeled with soft distance restraints on the double and single bond. The distances used for this modeling were taken from the mean values found for 15 vinylbenzyl entries in the Cambridge Structural Database <sup>67</sup> (data collection temperature between 160 and 190 K, R-factor below 0.07, and heaviest element Cl). Thermal similarity restraints were also applied to the carbon atoms in the vinyl groups for modeling.

The Squeeze procedure<sup>77</sup> was used to model the contributions of the solvent electron density to the total scattering. The atoms of the remaining solvent molecules were refined with isotropic atomic displacement parameters. Many of the H atoms were located in a difference map but repositioned geometrically. The H atoms were initially refined with soft restraints on the bond lengths and angles to regularize their geometry (C–H in the range 0.93–0.98 Å) and  $U_{\text{iso}}(\text{H})$  (in the range 1.2–1.5 times  $U_{\text{eq}}$  of the parent atom). Then, the positions were refined with riding constraints<sup>78</sup> and other hydrogen atoms were positioned geometrically.

The root-mean-square deviation of atomic position values of the clusters were calculated using Mercury<sup>79</sup>. Voids were also calculated using contact surface maps with a probe of 1.2 Å radius and a grid spacing of 1 Å. These voids give an estimate of the volume that could be filled by solvent or guest molecules<sup>80</sup>.

CCDC 1983366–1983368 contain supplementary crystallographic data for this paper. These data may be obtained free of charge from The Cambridge Crystallographic Data Centre via [http://www.ccdc.cam.ac.uk/data\\_request/cif](http://www.ccdc.cam.ac.uk/data_request/cif).

## ASSOCIATED CONTENT

### Supporting Information

The Supporting Information is available free of charge on the ACS Publications website.

- Crystallographic information files for styryl-functionalised T<sub>8</sub>, T<sub>10</sub> and T<sub>12</sub> POSS (CIF)
- Crystallographic, MALDI-TOF mass spectra and IR spectra and corresponding band assignments for styryl-functionalized T<sub>8</sub>, T<sub>10</sub>, and T<sub>12</sub> POSS (PDF)

## AUTHOR INFORMATION

### Corresponding Author

John R. Bartlett: E-mail: [j.bartlett@westernsydney.edu.au](mailto:j.bartlett@westernsydney.edu.au).  
ORCID: 0000-0001-6509-6160

Masafumi Unno: E-mail: [unno@gunma-u.ac.jp](mailto:unno@gunma-u.ac.jp).  
ORCID: 0000-0003-2158-1644

Michel Wong Chi Man: E-mail: [Michel.wong-chi-man@en-scm.fr](mailto:Michel.wong-chi-man@en-scm.fr).  
ORCID: 0000-0003-1390-4239

### Notes

The authors declare no competing financial interests.

## ACKNOWLEDGMENT

The authors gratefully acknowledge helpful discussions with Dr Guillaume Toquer (ICSM, University of Montpellier, CEA, CNRS, ENSCM, Marcoule, France). Funding from the French *Ministère de l'Enseignement Supérieur et de la Recherche* to support the PhD scholarship of ML, together with travel funding from the *Japan Student Services Organization*, is also gratefully acknowledged.

## REFERENCES

1. Scott, D. W., Thermal Rearrangement of Branched-Chain Methylpolysiloxanes. *J. Am. Chem. Soc.* **1946**, *68* (3), 356–358.
2. Barry, A. J.; Daudt, W. H.; Domicone, J. J.; Gilkey, J. W., Crystalline Organosilsesquioxanes. *J. Am. Chem. Soc.* **1955**, *77* (16), 4248–4252.
3. Cordes, D. B.; Lickiss, P. D.; Rataboul, F., Recent developments in the chemistry of cubic polyhedral oligosilsesquioxanes. *Chem. Rev.* **2010**, *110* (4), 2081–2173.
4. Laine, R. M., Nanobuilding blocks based on the [OSiO1.5]<sub>x</sub> (x = 6, 8, 10) octasilsesquioxanes. *J. Mater. Chem.* **2005**, *15* (35–36), 3725–3744.
5. Harrison, P. G.; Kannengiesser, R., Porous materials derived from trigonal-prismatic {Si6O9} and cubane {Si8O12} cage monomers. *Chem. Commun.* **1996**, (3), 415–416.
6. Zhang, C.; Babonneau, F.; Bonhomme, C.; Laine, R. M.; Soles, C. L.; Hristov, H. A.; Yee, A. F., Highly porous polyhedral silsesquioxane polymers. Synthesis and characterization. *J. Am. Chem. Soc.* **1998**, *120* (33), 8380–8391.
7. Morrison, J. J.; Love, C. J.; Manson, B. W.; Shannon, I. J.; Morris, R. E., Synthesis of functionalised porous network silsesquioxane polymers. *J. Mater. Chem.* **2002**, *12* (11), 3208–3212.
8. Wang, D.; Xue, L.; Li, L.; Deng, B.; Feng, S.; Liu, H.; Zhao, X., Rational design and synthesis of hybrid porous polymers derived from polyhedral oligomeric silsesquioxanes via heck coupling reactions. *Macromol. Rapid Commun.* **2013**, *34* (10), 861–866.
9. Akbari, A.; Arsalani, N.; Amini, M.; Jabbari, E., Cube-octameric silsesquioxane-mediated cargo copper Schiff base for efficient click reaction in aqueous media. *J. Mol. Catal. A Chem.* **2016**, *414*, 47–54.
10. Köytepe, S.; Demirel, M. H.; Gültek, A.; Seçkin, T., Metallo-supramolecular materials based on terpyridine-functionalized polyhedral silsesquioxane. *Polym. Int.* **2014**, *63* (4), 778–787.
11. Kowalewska, A., Self-assembling polyhedral silsesquioxanes - Structure and properties. *Curr. Org. Chem.* **2017**, *21* (14), 1243–1264.
12. Seino, M.; Wang, W.; Lofgreen, J. E.; Puzzo, D. P.; Manabe, T.; Ozin, G. A., Low-k periodic mesoporous organosilica with air walls: POSS-PMO. *J. Am. Chem. Soc.* **2011**, *133* (45), 18082–18085.
13. Kausar, A., State-of-the-Art Overview on Polymer/POSS Nanocomposite. *Polym.-Plast. Technol. Eng.* **2017**, *56* (13), 1401–1420.
14. Zhou, H.; Ye, Q.; Xu, J., Polyhedral oligomeric silsesquioxane-based hybrid materials and their applications. *Mater. Chem. Front.* **2017**, *1* (2), 212–230.
15. Chiacchio, M. A.; Borrello, L.; Di Pasquale, G.; Pollicino, A.; Bottino, F. A.; Rescifina, A., Synthesis of functionalized polyhedral oligomeric silsesquioxane (POSS) macromers by microwave assisted 1,3-dipolar cycloaddition. *Tetrahedron* **2005**, *61* (33), 7986–7993.
16. Haddad, T. S.; Viers, B. D.; Phillips, S. H., Polyhedral oligomeric silsesquioxane (POSS)-styrene macromers. *J. Inorg. Organomet. Polym.* **2001**, *11* (3), 155–164.
17. Phillips, S. H.; Haddad, T. S.; Tomczak, S. J., Developments in nanoscience: Polyhedral oligomeric silsesquioxane (POSS)-polymers. *Curr. Opin. Solid State Mater. Sci.* **2004**, *8* (1), 21–29.

18. Romo-Urbe, A.; Mather, P. T.; Haddad, T. S.; Lichtenhan, J. D., Viscoelastic and morphological behavior of hybrid styryl-based polyhedral oligomeric silsesquioxane (POSS) copolymers. *J Polym Sci Part B* **1998**, *36* (11), 1857-1872.
19. Bassindale, A. R.; Pourny, M.; Taylor, P. G.; Hursthouse, M. B.; Light, M. E., Fluoride-ion encapsulation within a silsesquioxane cage. *Angew. Chem. Int. Ed.* **2003**, *42* (30), 3487-3490.
20. Clegg, W.; Sheldrick, G. M.; Vater, N., Dodeca(phenylsilsesquioxane). *Acta Crystallogr., Sect. B* **1980**, *B36* (12), 3162-3164.
21. Gnanasekaran, D.; Madhavpan, K.; Reddy, R. S. R., Developments of polyhedral oligomeric silsesquioxanes (POSS), POSS nanocomposites and their applications: A review. *J. Sci. Ind. Res.* **2009**, *68* (6), 437-464.
22. Kannan, R. Y.; Salacinski, H. J.; Butler, P. E.; Seifalian, A. M., Polyhedral oligomeric silsesquioxane nanocomposites: The next generation material for biomedical applications. *Acc. Chem. Res.* **2005**, *38* (11), 879-884.
23. Ghanbari, H.; Cousins, B. G.; Seifalian, A. M., A nanocage for nanomedicine: Polyhedral oligomeric silsesquioxane (POSS). *Macromol. Rapid Commun.* **2011**, *32* (14), 1032-1046.
24. Solouk, A.; Cousins, B. G.; Mirahmadi, F.; Mirzadeh, H.; Nadoushan, M. R. J.; Shokrgozar, M. A.; Seifalian, A. M., Biomimetic modified clinical-grade POSS-PCU nanocomposite polymer for bypass graft applications: A preliminary assessment of endothelial cell adhesion and haemocompatibility. *Mater. Sci. Eng. C* **2015**, *46*, 400-408.
25. Nayyer, L.; Birchall, M.; Seifalian, A. M.; Jell, G., Design and development of nanocomposite scaffolds for auricular reconstruction. *Nanomed. Nanotechnol. Biol. Med.* **2014**, *10* (1), 235-246.
26. Kannan, R. Y.; Salacinski, H. J.; De Groot, J.; Clatworthy, I.; Bozec, L.; Horton, M.; Butler, P. E.; Seifalian, A. M., The antithrombogenic potential of a polyhedral oligomeric silsesquioxane (POSS) nanocomposite. *Biomacromolecules* **2006**, *7* (1), 215-223.
27. Kannan, R. Y.; Salacinski, H. J.; Odlyha, M.; Butler, P. E.; Seifalian, A. M., The degradative resistance of polyhedral oligomeric silsesquioxane nanocore integrated polyurethanes: An in vitro study. *Biomaterials* **2006**, *27* (9), 1971-1979.
28. Quadrelli, E. A.; Basset, J. M., On silsesquioxanes' accuracy as molecular models for silica-grafted complexes in heterogeneous catalysis. *Coord. Chem. Rev.* **2010**, *254* (5-6), 707-728.
29. Giacalone, F.; Gruttadauria, M., Covalently Supported Ionic Liquid Phases: An Advanced Class of Recyclable Catalytic Systems. *ChemCatChem* **2016**, *8* (4), 664-684.
30. Bivona, L. A.; Giacalone, F.; Carbonell, E.; Gruttadauria, M.; Aprile, C., Proximity Effect using a Nanocage Structure: Polyhedral Oligomeric Silsesquioxane-Imidazolium Tetrachloro- palladate Salt as a Precatalyst for the Suzuki-Miyaura Reaction in Water. *ChemCatChem* **2016**, *8* (9), 1685-1691.
31. Zhou, Y.; Yang, G.; Lu, C.; Nie, J.; Chen, Z.; Ren, J., POSS supported C<sub>2</sub>-symmetric bisprolinamide as a recyclable chiral catalyst for asymmetric Aldol reaction. *Catal. Commun.* **2016**, *75*, 23-27.
32. Chanmungkalakul, S.; Ervithayasuporn, V.; Boonkitti, P.; Phuekphong, A.; Prigyai, N.; Kladsomboon, S.; Kiatkamjornwong, S., Anion identification using silsesquioxane cages. *Chem. Sci.* **2018**, *9* (40), 7753-7765.
33. Chanmungkalakul, S.; Ervithayasuporn, V.; Hanprasit, S.; Masik, M.; Prigyai, N.; Kiatkamjornwong, S., Silsesquioxane cages as fluoride sensors. *Chem. Commun.* **2017**, *53* (89), 12108-12111.
34. Li, Z.; Kong, J.; Wang, F.; He, C., Polyhedral oligomeric silsesquioxanes (POSSs): An important building block for organic optoelectronic materials. *J. Mater. Chem. C* **2017**, *5* (22), 5283-5298.
35. Ervithayasuporn, V.; Kwanplod, K.; Boonmak, J.; Youngme, S.; Sangtrirutnugul, P., Homogeneous and heterogeneous catalysts of organopalladium functionalized-polyhedral oligomeric silsesquioxanes for Suzuki-Miyaura reaction. *J. Catal.* **2015**, *332*, 62-69.
36. Feng, X.; Zhu, S.; Yue, K.; Su, H.; Guo, K.; Wesdemiotis, C.; Zhang, W. B.; Cheng, S. Z. D.; Li, Y., T10 polyhedral oligomeric silsesquioxane-based shape amphiphiles with diverse head functionalities via "click" chemistry. *ACS Macro Lett.* **2014**, *3* (9), 900-905.
37. Ervithayasuporn, V.; Chimjarn, S., Synthesis and isolation of methacrylate- and acrylate-functionalized polyhedral oligomeric silsesquioxanes (T8, T10, and T12) and characterization of the relationship between their chemical structures and physical properties. *Inorg. Chem.* **2013**, *52* (22), 13108-13112.
38. Chimjarn, S.; Kunthom, R.; Chancharone, P.; Sodkhomkhum, R.; Sangtrirutnugul, P.; Ervithayasuporn, V., Synthesis of aromatic functionalized cage-rearranged silsesquioxanes (T8, T10, and T12) via nucleophilic substitution reactions. *Dalton Trans.* **2014**, *44* (3), 916-919.
39. Janeta, M.; John, L.; Ejfler, J.; Szafert, S., Novel organic-inorganic hybrids based on T8 and T10 silsesquioxanes: Synthesis, cage-rearrangement and properties. *RSC Adv.* **2015**, *5* (88), 72340-72351.
40. Brown, J. F., Jr.; Vogt, L. H., Jr.; PreScott, P. I., Preparation and Characterization of the Lower Equilibrated Phenylsilsesquioxanes. *J. Am. Chem. Soc.* **1964**, *86* (6), 1120-1125.
41. Furgal, J. C.; Goodson, T., III; Laine, R. M., D5h [PhSiO<sub>1.5</sub>]<sub>10</sub> synthesis via F- catalyzed rearrangement of [PhSiO<sub>1.5</sub>]<sub>n</sub>. An experimental/computational analysis of likely reaction pathways. *Dalton Trans.* **2016**, *45* (3), 1025-1039.
42. Roll, M. F.; Kampf, J. W.; Kim, Y.; Yi, E.; Laine, R. M., Nano building blocks via iodination of [PhSiO<sub>1.5</sub>]<sub>n</sub>, forming [p-I-C<sub>6</sub>H<sub>4</sub>SiO<sub>1.5</sub>]<sub>n</sub> (n = 8, 10, 12), and a new route to high-surface-area, thermally stable, microporous materials via thermal elimination of I<sub>2</sub>. *J. Am. Chem. Soc.* **2010**, *132* (29), 10171-10183.
43. Miyazato, A.; Pakjamsai, C.; Kawakami, Y., Octa, deca, and dodeca(4-nitrophenyl) cage silsesquioxanes via 4-trimethylsilylphenyl derivatives. *Dalton Trans.* **2010**, *39* (13), 3239-3244.
44. Hwan Jung, J.; Furgal, J. C.; Goodson, T.; Mizumo, T.; Schwartz, M.; Chou, K.; Vonet, J. F.; Laine, R. M., 3-D molecular mixtures of catalytically functionalized [vinylSiO<sub>1.5</sub>]<sub>10</sub>/[vinylSiO<sub>1.5</sub>]<sub>12</sub>. Photophysical characterization of second generation derivatives. *Chem. Mater.* **2012**, *24* (10), 1883-1895.
45. Kawakami, Y.; Yamaguchi, K.; Yokozawa, T.; Serizawa, T.; Hasegawa, M.; Kabe, Y., Higher polyhedral silsesquioxane (POSS) cage by amine-catalyzed condensation

- of silanols and related siloxanes. *Chem. Lett.* **2007**, *36* (6), 792-793.
46. Rikowski, E.; Marsmann, H. C., Cage-rearrangement of silsesquioxanes. *Polyhedron* **1997**, *16* (19), 3357-3361.
47. Imai, K.; Kaneko, Y., Preparation of Ammonium-Functionalized Polyhedral Oligomeric Silsesquioxanes with High Proportions of Cage-like Decamer and Their Facile Separation. *Inorg. Chem.* **2017**, *56* (7), 4133-4140.
48. Matsumoto, T.; Kaneko, Y., Selective and high-yielding preparation of ammonium-functionalized cage-like octasilsesquioxanes using superacid catalyst in dimethyl sulfoxide. *Chem. Lett.* **2018**, *47* (7), 864-867.
49. Ervithayasuporn, V.; Wang, X.; Kawakami, Y., Synthesis and characterization of highly pure azido-functionalized polyhedral oligomeric silsesquioxanes (POSS). *Chem. Commun.* **2009**, (34), 5130-5132.
50. Asuncion, M. Z.; Laine, R. M., Fluoride rearrangement reactions of polyphenyl- and polyvinylsilsesquioxanes as a facile route to mixed functional phenyl, vinyl T10 and T12 Silsesquioxanes. *J. Am. Chem. Soc.* **2010**, *132* (11), 3723-3736.
51. Fasce, D. P.; Williams, R. J. J.; Méchin, F.; Pascault, J. P.; Llauro, M. F.; Pétaud, R., Synthesis and characterization of polyhedral silsesquioxanes bearing bulky functionalized substituents. *Macromolecules* **1999**, *32* (15), 4757-4763.
52. Itami, Y.; Marciniak, B.; Kabicki, M., Functionalization of Octavinylsilsesquioxane by Ruthenium-Catalyzed Silylative Coupling versus Cross-Metathesis. *Chem. Eur. J.* **2004**, *10* (5), 1239-1248.
53. Anderson, S. E.; Bodzin, D. J.; Haddad, T. S.; Boatz, J. A.; Mabry, J. M.; Mitchell, C.; Bowers, M. T., Structural investigation of encapsulated fluoride in polyhedral oligomeric silsesquioxane cages using ion mobility mass spectrometry and molecular mechanics. *Chem. Mater.* **2008**, *20* (13), 4299-4309.
54. Guenther, A. J.; Lamison, K. R.; Lubin, L. M.; Haddad, T. S.; Mabry, J. M., Hansen solubility parameters for octahedral oligomeric silsesquioxanes. *Ind. Eng. Chem. Res.* **2012**, *51* (38), 12282-12293.
55. Zhang, H. X.; Lee, H. Y.; Shin, Y. J.; Lee, D. H.; Noh, S. K., Notes: Effect of 3rd monomer addition on styrene/styryl-polyhedral oligomeric silsesquioxane (POSS) copolymerization. *Macromol. Res.* **2009**, *17* (5), 352-355.
56. Anderson, S. E.; Somogyi, A.; Haddad, T. S.; Coughlin, E. B.; Gadodia, G.; Marten, D. F.; Ray, J.; Bowers, M. T., ESI and MALDI mass spectrometry of large POSS oligomers. *Int. J. Mass Spectrom.* **2010**, *292* (1-3), 38-47.
57. Wada, K.; Watanabe, K.; Yamamoto, K. Resin composition for forming dielectric films with good Young's modulus. WO2010067683A1, 2010.
58. Bassindale, A. R.; Liu, Z.; MacKinnon, I. A.; Taylor, P. G.; Yang, Y.; Light, M. E.; Horton, P. N.; Hursthouse, M. B., A higher yielding route for T8 silsesquioxane cages and X-ray crystal structures of some novel spherosilicates. *Dalton Trans.* **2003**, (14), 2945-2949.
59. Agaskar, P. A., New Synthetic Route to the Hydridospherosiloxanes Oh-H8Si8O12 and D5h-H10Si10O15. *Inorg. Chem.* **1991**, *30* (13), 2707-2708.
60. Xu, H.; Yang, B.; Gao, X.; Li, C.; Guang, S., Synthesis and characterization of organic-inorganic hybrid polymers with a well-defined structure from diamines and epoxy-functionalized polyhedral oligomeric silsesquioxanes. *J. Appl. Polym. Sci.* **2006**, *101* (6), 3730-3735.
61. Bassindale, A. R.; Chen, H.; Liu, Z.; MacKinnon, I. A.; Parker, D. J.; Taylor, P. G.; Yang, Y.; Light, M. E.; Horton, P. N.; Hursthouse, M. B., A higher yielding route to octasilsesquioxane cages using tetrabutylammonium fluoride, Part 2: Further synthetic advances, mechanistic investigations and X-ray crystal structure studies into the factors that determine cage geometry in the solid state. *J. Organomet. Chem.* **2004**, *689* (21), 3287-3300.
62. Koželj, M.; Orel, B., Synthesis of polyhedral phenylsilsesquioxanes with KF as the source of the fluoride ion. *Dalton Trans.* **2008**, (37), 5072-5075.
63. Hossain, M. A.; Hursthouse, M. B.; Malik, K. M. A., Octa(phenylsilsesquioxane) acetone solvate. *Acta Crystallogr., Sect. B* **1979**, *B35* (9), 2258-60.
64. Calzaferri, G.; Marcolli, C.; Imhof, R.; Törnroos, K. W., The monophenylhydrosilsesquioxanes PhHn-1SiO1.5n where n = 8 or 10. *Journal of the Chemical Society - Dalton Transactions* **1996**, (15), 3313-3322.
65. Bürgi, H. B.; Toernroos, K. W.; Calzaferri, G.; Bürgy, H., X-ray diffraction study of the molecular structure of a spherohydrosilsesquioxane, H10Si10O15, a flexible assembly of rigid tetrahedra. *Inorg. Chem.* **1993**, *32* (22), 4914-19.
66. Marcolli, C.; Lainé, P.; Bühler, R.; Calzaferri, G.; Tomkinson, J., Vibrations of H8Si8O12, D8Si8O12, and H10Si10O15 as determined by INS, IR, and Raman experiments. *J Phys Chem B* **1997**, *101* (7), 1171-1179.
67. Groom, C. R.; Bruno, I. J.; Lightfoot, M. P.; Ward, S. C., The Cambridge structural database. *Acta Crystallogr. Sect. B Struct. Sci. Cryst. Eng. Mater.* **2016**, *72* (2), 171-179.
68. Agaskar, P. A.; Klemperer, W. G., The higher hydridospherosiloxanes: synthesis and structures of HnSinO1.5n (n = 12, 14, 16, 18). *Inorg. Chim. Acta* **1995**, *229* (1-2), 355-364.
69. Törnroos, K. W.; Bürgi, H. B.; Calzaferri, G.; Bürgy, H., The crystal and molecular structure of dodecahydrosilsesquioxane, H12Si12O18. *Acta Crystallogr. Sect. B Struct. Sci.* **1995**, *51* (2), 155-161.
70. Hoque, M. A.; Cho, Y. H.; Kawakami, Y., High performance holographic gratings formed with novel photopolymer films containing hyper-branched silsesquioxane. *React Funct Polym* **2007**, *67* (11 SPEC. ISS.), 1192-1199.
71. Lausi, A.; Polentarutti, M.; Onesti, S.; Plaisier, J. R.; Busetto, E.; Bais, G.; Barba, L.; Cassetta, A.; Campi, G.; Lamba, D.; Pifferi, A.; Mande, S. C.; Sarma, D. D.; Sharma, S. M.; Paolucci, G., Status of the crystallography beamlines at Elettra. *Eur. Phys. J. Plus* **2015**, *130* (3), Article number 43, 8p.
72. Kabsch, W., XDS. *Acta Crystallogr. Sect. D Biol. Crystallogr.* **2010**, *66* (2), 125-132.
73. Winn, M. D.; Ballard, C. C.; Cowtan, K. D.; Dodson, E. J.; Emsley, P.; Evans, P. R.; Keegan, R. M.; Krissinel, E. B.; Leslie, A. G. W.; McCoy, A.; McNicholas, S. J.; Murshudov, G. N.; Pannu, N. S.; Potterton, E. A.; Powell, H. R.; Read, R. J.; Vagin, A.; Wilson, K. S., Overview of the CCP4 suite and current developments. *Acta Crystallogr. Sect. D Biol. Crystallogr.* **2011**, *67* (4), 235-242.
74. Van Der Lee, A., Charge flipping for routine structure solution. *J. Appl. Crystallog.* **2013**, *46* (5), 1306-1315.
75. Palatinus, L.; Chapuis, G., SUPERFLIP - A computer program for the solution of crystal structures by charge flipping in arbitrary dimensions. *J. Appl. Crystallog.* **2007**, *40* (4), 786-790.
76. Betteridge, P. W.; Carruthers, J. R.; Cooper, R. I.; Prout, K.; Watkin, D. J., CRYSTALS version 12: software for guided

crystal structure analysis. *J. Appl. Crystallog.* **2003**, *36*, 1487-1487.

77. Spek, A. L., PLATON SQUEEZE: A tool for the calculation of the disordered solvent contribution to the calculated structure factors. *Acta crystallogr., C Struct. Chem.* **2015**, *71*, 9-18.

78. Cooper, R. I.; Thompson, A. L.; Watkin, D. J., CRYSTALS enhancements: Dealing with hydrogen atoms in refinement. *J. Appl. Crystallog.* **2010**, *43* (5 PART 1), 1100-1107.

79. Macrae, C. F.; Bruno, I. J.; Chisholm, J. A.; Edgington, P. R.; McCabe, P.; Pidcock, E.; Rodriguez-Monge, L.; Taylor, R.; Van De Streek, J.; Wood, P. A., Mercury CSD 2.0 - New features for the visualization and investigation of crystal structures. *J. Appl. Crystallog.* **2008**, *41* (2), 466-470.

80. Barbour, L. J., Crystal porosity and the burden of proof. *Chem. Commun.* **2006**, (11), 1163-1168.

Insert Table of Contents artwork here

